CHEMISTRY OF MATERIALS

Article

pubs.acs.org/cm

Electronic Structure of Tantalum Oxynitride Perovskite Photocatalysts

Snjezana Balaz,*[,†] Spencer H. Porter,[‡] Patrick M. Woodward,[‡,§] and Leonard J. Brillson[†,§]

[†]Department of Electrical and Computer Engineering, The Ohio State University, Columbus, Ohio 43210, United States

[‡]Department of Chemistry, The Ohio State University, Columbus, Ohio 43210, United States

[§]Department of Physics, The Ohio State University, Columbus, Ohio 43210, United States

ABSTRACT: The tantalum oxynitride perovskites $ATaO_2N$ (A = Ca, Sr, and Ba) and $PrTaON_2$ are promising candidates for the photocatalytic splitting of water under illumination with visible light. A combination of X-ray photoemission spectroscopy (XPS), Kelvin probe force microscopy (KPFM), UV−vis spectroscopy, and depth-resolved cathodoluminescence spectroscopy (DRCLS) has been used to determine the absolute conduction and valence band energy levels of these four compounds. All have conduction band edges that lie above the reduction potential for water and therefore are suitable for the photocatalytic production of hydrogen, whereas the valence band edges lie near the oxidation potential of water. The position of the conduction band edge is closely linked to the Ta−O/N−Ta bond angles and hence tilting of the octahedra, whereas the position of the valence band edge is more sensitive to the oxygen-to-nitrogen ratio.

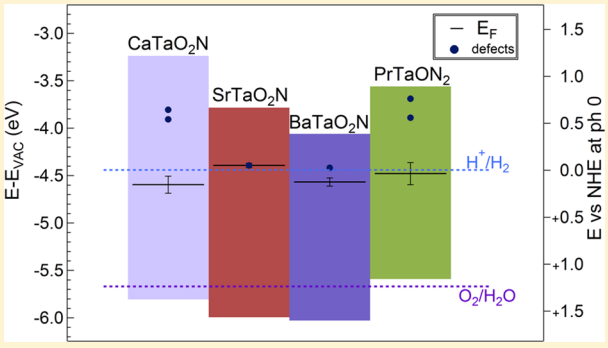

KEYWORDS: *tantalum oxynitride perovskite, electronic structure, photocatalysts, water splitting, conduction band, valence band, defects, AFM, KPFM, XRD, XPS, DRCLS, UV−vis, $CaTaO_2N$, $SrTaO_2N$, $BaTaO_2N$, $PrTaON_2$*

1. INTRODUCTION

The photocatalysis of water represents a fundamental mechanism for the production of hydrogen as a clean and renewable energy source.[1,2] First demonstrated with a photoelectrochemical cell in 1972,[3] the photocatalysis of water involves the absorption of a photon to create an electron−hole pair. The electron and hole must then be separated and independently migrate to the surface of the semiconductor where the electron can reduce water to produce hydrogen and the hole can oxidize water to produce oxygen. For these reactions to occur, the conduction band edge needs to be above the reduction potential of water ($2\,H^+(aq) + 2\,e^- \rightarrow H_2(g)$, E° = 0 V vs standard hydrogen electrode (SHE)), and the valence band edge must be below the oxidation potential of water ($H_2O(l) + 4h^+ \rightarrow O_2(g) + 4\,H^+(aq)$, $E^\circ = -1.23$ V vs SHE).[4,5] In theory, a semiconductor with a band gap as small as 1.3 eV could drive water splitting if the band edges were ideally positioned, no overpotentials were required, and the surface of the semiconductor was photochemically stable.

TiO_2 is the archetypal inorganic photocatalyst. Its valence and conduction bands are positioned so that water splitting can occur, and it is photochemically stable. However, the 3.2 eV band gap of TiO_2 (anatase form) is much larger than the minimum needed for water splitting, largely because its valence band is positioned well below the oxidation potential of water. The large band gap means that only a very small portion of the solar spectrum can be absorbed. The discovery of a photocatalyst capable of harvesting a significant portion of the solar spectrum while retaining the stability and efficiency of TiO_2 would be a transformative breakthrough.

The tantalum oxynitride perovskites, $ATaO_2N$ (A = Ca, Sr, and Ba) and $PrTaON_2$, are promising candidates for the photocatalytic splitting of water under illumination with visible light. They have smaller band gaps than TiO_2 (1.5−2.5 eV) and are stable in aqueous solutions, and the presence of tantalum offers the promise of high efficiency because many of the highest quantum efficiency photocatalysts contain tantalum (e.g., $K_3Ta_3B_2O_{12}$,[6] $NaTaO_3$,[7,8] Ta_2O_5,[9] $Sr_2Ta_2O_7$,[10] and $Ba_5Ta_4O_{15}$[11]). Unfortunately, the quantum efficiencies of the perovskite oxynitrides have so far been quite low.[1,4,12−20,31,42] There are two factors that are potentially responsible for the low quantum efficiencies: (1) the poor band alignment of the valence and conduction band edges with respect to the water redox potentials and (2) the presence of recombination centers that prevent photogenerated carriers from driving the photocatalytic process.

Although there have been prior studies that report band gaps for $CaTaO_2N$, $SrTaO_2N$, and $BaTaO_2N$,[21,22] the absolute band positions are not known. Furthermore, there have been no reports of the presence or energy levels of the defect states. Our aim in this study is to determine the absolute energy levels of the oxynitride band edges, to assess their intrinsic potential as

Received: June 4, 2013
Revised: July 16, 2013
Published: July 17, 2013

photocatalysts, and to determine the energy levels of the defect states that can act as recombination centers and degrade photocatalytic performance.

2. EXPERIMENTAL METHODS

Synthesis. Samples of $CaTaO_2N$, $SrTaO_2N$, and $PrTaON_2$ were synthesized by a methanol (MeOH) coprecipitation method. Here, $CaCl_2{\cdot}4H_2O$ (99+%, JT Baker), $SrCl_2{\cdot}4H_2O$ (99%, Aldrich), or $PrCl_3$ (anhydrous, 99.99%, Sigma Aldrich) was added in an equimolar amount to $TaCl_5$ (99.99%, Alfa Aesar) solvated in methanol (anhydrous, 99.8%, Mallinckrodt) to create 4.7×10^{-2} M solutions (e.g., 1.4×10^{-3} mol of metal salt was added to 30 mL of solvent). The metal ions were precipitated by adding a concentrated NH_4OH solution dropwise while the solution was rapidly stirred. The precipitate was dried by heating at 130 °C overnight. This precursor was converted to an oxynitride by heating in flowing ammonia at 800–850 °C for 18–24 h. The powdered oxynitride was suspended in an acetone/water mixture and allowed to evaporate to dryness onto a tungsten substrate placed at the bottom of the suspension vessel. A final heating at 450 °C for 0.5 h under nitrogen was carried out to remove the residual organic material and aid the film integrity.

$BaTaO_2N$ was prepared by a conventional solid-state reaction. Here, $BaCO_3$ (Grade 1, Johnson Matthey) and Ta_2O_5 (99.993%, Alfa Aesar) were ground together for 30 min using a mortar and pestle. The resulting powder was heated in flowing ammonia at 950 °C for 24 h. The resultant oxynitride powder was suspended in an acetone/water mixture and allowed to evaporate to dryness on a tungsten substrate. A final heating at 450 °C for 0.5 h under nitrogen was carried out to remove the residual organic content. Attempts to make a $BaTaO_2N$ film that was phase pure by solution methods were unsuccessful, which is a result that has been reported elsewhere in the literature.[23]

X-ray powder diffraction (XRPD) patterns were collected on a Bruker D8 diffractometer (40 kV/50 mA/Cu Kα1) equipped with a Ge ⟨111⟩ monochromator and a Lynx-eye detector to confirm the phase purity. Typical parameters used for the XRPD scans were a range of 10–110° 2θ with a 0.015° step size and a 0.75 s dwell time. Rietveld refinements were completed using the Topas Academic software.

Measurements of the Electronic Structure. Several complementary, atomic-scale electronic and morphological techniques were employed to characterize the electronic structures of these oxynitrides: (1) X-ray photoemission spectroscopy (XPS) to determine the valence band edge position, E_V, relative to the Fermi level, E_F; (2) Kelvin probe force microscopy (KPFM) to determine E_F relative to E_{VAC} and thereby E_V relative to E_{VAC}; (3) UV–vis diffuse reflectance as an independent method of determining E_G and thereby E_C relative to E_V and E_{VAC}; and (4) depth-resolved cathodoluminescence spectroscopy (DRCLS) to determine the band gap, E_G. These results provide the conduction and valence band edges and their variations across this series.

XPS core levels and valence band spectra were acquired at room temperature using a PHI 5000 VersaProbe. We corrected the valence band energies for any charging by calibrating the binding energy of C1s to 284.9 eV, which is the value measured for $BaTaO_2N$, whose thin films did not charge and whose C1s binding energy was obtained while acquiring the valence spectra. A Park XE-70 AFM/KPFM in noncontact mode provided simultaneous topography (noise floor <0.05 nm) and electric potential maps at room temperature in air. We extracted work functions from the contact potential difference (CPD) between the oxynitride surface and the AFM/KPFM tip. CPD values were compared with that of highly oriented pyroltyic graphite (HOPG), which is stable in both vacuum and air and has a work function of 4.475 eV.[33] UV–vis diffuse reflectance data were collected using an Ocean Optics USB4000 UV–vis spectrometer equipped with standard reflectance probe and a DH-2000-BAL deuterium/tungsten halogen source.

DRCLS measurements were performed in an ultra-high-vacuum (UHV) chamber (base pressure 5×10^{-10} Torr) using a glancing incidence electron gun and collection optics to acquire optical spectra across the near-IR to UV wavelength range. In DRLCS, radiative recombination occurs between band edges and gap states. For a more detailed description of this technique, see, for example, refs 25 and 26. Oxynitride samples were cooled by a helium cryotip and copper braid to ~80 K. The incident electron beam energies, E_B, varied from 0.5 to 5 keV at a constant power of 2 mW.

With DRCLS, we are able to measure not only the band gap energies, E_G, but also the energies of the defect states within the band gap. Furthermore, by varying the incident beam energy, E_B, we are able to measure both quantities as a function of the depth. It is possible to calibrate the depth of cathodoluminescence excitation on a nanometer scale using Monte Carlo simulations[29] that determine the rate of the energy loss of the electron cascade generated by the incident electron beam as a function of E_B, sample density, and atomic mass.[24−26] The Bohr–Bethe range, R_B, of the maximum excitation depth and the depth of the peak rate of excitation, U_0, both increase with increasing incident beam energy, E_B. This nanometer-scale control of the excitation depth is useful for the oxynitrides for two reasons. First, we were able to measure the electronic features that were characteristic of the oxynitride and not of the substrate below. Indeed, DRCLS permits studies of films that are only nanometers thick.[27,28] Second, a comparison of DRCL spectra for near-surface versus bulk excitation could reveal how uniform the films were, especially whether any surface electronic changes take place that differ from the bulk properties. Thus, for E_B = 1 keV in $CaTaO_2N$, electron–hole pair creation and luminescence reaches a maximum at ~14 nm, whereas it peaks at ~126 nm for E_B = 5 keV. Similarly, in $SrTaO_2N$, $BaTaO_2N$, and $PrTaON_2$, an E_B value of 1 keV probes ~13, ~ 14, and ~14 nm, respectively, whereas 5 keV probes ~117, ~106, and ~134 nm, respectively.

Extensive XPS, KPFM, and DRCLS measurements revealed that the film properties depended sensitively on the deposition conditions. Therefore, we used atomic force microscopy (AFM) to measure the film surface morphology. We established several criteria for obtaining films with physical properties that were characteristic of each oxynitride. A primary requirement was that the sample should have relatively smooth surfaces and full substrate coverage as measured by AFM. We did not include measurements of the samples that exhibited nonuniform coverage. Another criterion was that the sample should have minimal or no charging during the KPFM and XPS measurements. We utilized AFM/KPFM to locate the characteristic surface areas with the smoothest morphology and lowest charging. We followed the same procedures for synthesizing different compounds by the same technique. The results presented here were obtained from only samples that satisfied all of these criteria.

3. RESULTS

X-ray powder diffraction (XRPD) patterns for all four samples are shown in Figure 1. The black tick marks denote the indexed peak positions for each perovskite compound, whereas the red tick marks are associated with the peaks from the underlying tungsten substrate. Refinements of the XRPD patterns showed that $BaTaO_2N$, $SrTaO_2N$, and $CaTaO_2N$ have cubic, tetragonal, and orthorhombic symmetries, respectively, which is in agreement with earlier studies.[22] $PrTaON_2$ is orthorhombic and isostructural with $CaTaO_2N$. The structures are shown in Figure 2. All samples were phase pure, with the exception of $BaTaO_2N$, which contained a trace amount of Ta_3N_5. Rietveld refinements indicated that 4 mass % or 2.6 mol % Ta_3N_5 was present. The lattice parameters for the alkaline-earth tantalates agree well with literature reports for these compounds (Supporting Information). $PrTaO_2N$, which is reported here for the first time, is orthorhombic with *Pnma* space group symmetry and lattice parameters of a = 5.682(6), b = 8.030(8), and c = 5.681(7).

The colors of the resulting oxynitride powders were as follows: $CaTaO_2N$ is yellow, $SrTaO_2N$ is light orange,

dx.doi.org/10.1021/cm401815w | *Chem. Mater.* 2013, 25, 3337–3343

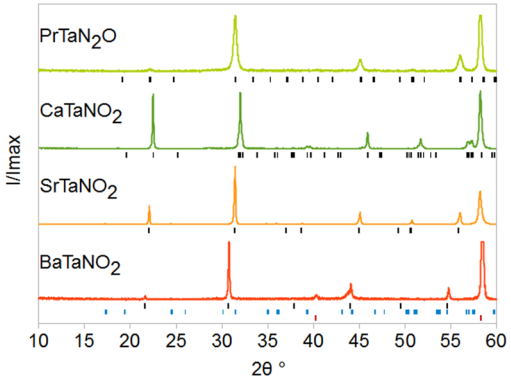

Figure 1. X-ray powder diffraction patterns of oxynitride films deposited on tungsten substrates. The black tick marks denote the peaks associated with the oxynitride perovskite, the red tick marks indicate the peaks associated with the tungsten substrate, and the blue tick marks indicate the peaks associated with Ta_3N_5.

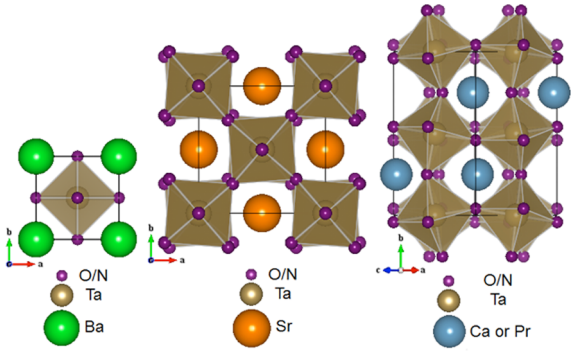

Figure 2. Structures of cubic $BaTaO_2N$, tetragonal $SrTaO_2N$, and orthorhombic $CaTaO_2N$ or $PrTaON_2$.

$BaTaO_2N$ is brick red-brown, and $PrTaON_2$ is maroon. The colors of the first three compounds are in good agreement with previous literature reports. Figure 3 shows characteristic UV–vis diffuse reflectance spectra for these compounds where the band gap energies were estimated by extrapolating the steep part of the absorption spectrum back to 0 absorbance. This approach yielded values of 2.6 eV for $CaTaO_2N$, 2.2 eV for $SrTaO_2N$, 2.0 eV for $BaTaO_2N$, and 2.0 eV for $PrTaON_2$. In each case, these values are slightly larger than previous reports: 1.8–1.9 eV for $BaTaO_2N$, 2.1 eV for $SrTaO_2N$, and 2.4 eV for $CaTaO_2N$.[21,22] No prior reports are available for $PrTaON_2$.

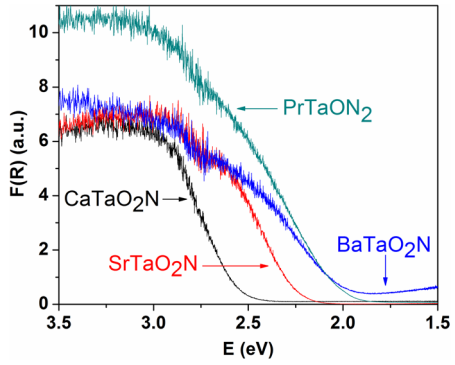

Figure 3. UV–vis spectra of $CaTaO_2N$, $SrTaO_2N$, $BaTaO_2N$, and $PrTaON_2$.

Levels of reduced tantalum (e.g., Ta^{4+}), even at the level of a few percent, will lead to sub-band gap absorption that will darken the compound and show up in the diffuse reflectance data. For $CaTaO_2N$, $SrTaO_2N$, and $PrTaON_2$, there is no sign of such absorption. This observation confirms the presence of Ta^{5+}, which when coupled with the observation that the lattice parameters are in close agreement with literature values leaves little doubt that the samples are quite close to their target stoichiometries. In contrast, $BaTaO_2N$ does absorb a small amount of light below the band gap. This cannot be attributed to the presence of a few percent Ta_3N_5 detected in this sample by XRPD because that compound has a band gap of 2.1 eV.[32,41] Instead, this likely indicates the presence of some reduced tantalum in this phase resulting from either anion vacancies or slight variations in the 2:1 ratio of oxygen to nitrogen.

Figure 4 shows AFM (left) and KPFM (right) maps of specimens synthesized by methods that yielded the lowest DRCLS defect emissions and the lowest XPS charging. AFM and KPFM are taken simultaneously over the same spot/area. The scans were taken over three or four spots for each sample (only one of which is shown in Figure 3) to check for uniformity. The resulting scans were very similar from one region to the next for all samples. The samples chosen for further analysis showed the least charging during KPFM measurements of CPD and possessed the smoothest surfaces, with an average roughness not exceeding 300 nm (Table 1) and an average height limited to 1 μm. We performed AFM/KPFM and DRCLS on all prepared samples. However, we acquired XPS data for only a subset of specimens that satisfied the morphological and charging criteria.

Using DRCL spectroscopy, we identified growth methods that yielded specimens with the lowest defect emission intensities relative to that of oxynitride's near band edge (NBE) emission intensity. This ratio is termed I(defect)/I(NBE). Figure 5 illustrates the DRCL spectra from the oxynitrides prepared by methods that yielded the lowest I(defect)/I(NBE) ratios. Each panel contains three or four spectra taken at E_B = 0.5 (where obtained), 1, 3, and 5 keV, corresponding to 6–7 (where obtained), 12–14, 44–65, and 98–134 nm excitation depths, respectively, as estimated with Monte Carlo simulations.[29] The DRCL spectra of $CaTaO_2N$, $SrTaO_2N$, and $PrTaON_2$ exhibit peaks that can be attributed to near band edge emissions at 2.57, 2.06, and 1.92 eV. These values are all quite close but slightly lower than the values estimated from the UV–vis spectra shown in Figure 3. It is not unusual that the near band edge emission would be 0.1 eV or so smaller than the full band gap because of recombination via excitons.[30]

The DRCL spectra show emissions at energies both below and above the band gap. The emissions with energies less than the band gap are associated with defects that produce states in the band gap that lead to radiative electron–hole recombination. The emissions with energies higher than the band gap are due to transitions between higher lying states above the conduction band minimum with the valence band.[31] The energies of these peak features range from 3.5 to near 6 eV with nearly identical 3.5 eV peaks but slightly different energies in the 4 to 5 eV range, which is consistent with their common Ta-derived conduction band features. In contrast, emissions at energies below the near band edge cannot be due to bulk features. The intensities of these sub-band gap defect states vary with respect to I(NBE), depending on the sample preparation and excitation depth.

dx.doi.org/10.1021/cm401815w | Chem. Mater. 2013, 25, 3337–3343

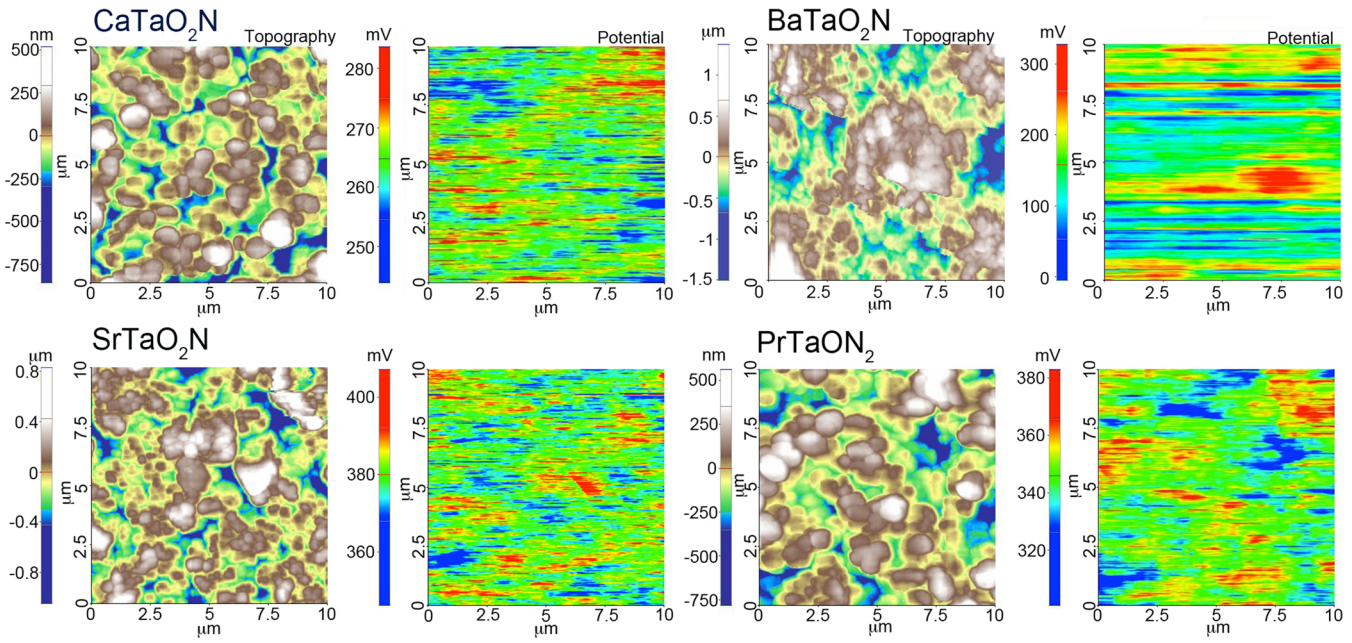

Figure 4. AFM (left) and KPFM (right) maps of the oxynitrides studied. The AFM shows the topography, and the KPFM shows the potential. KPFM potential variations across the surface are relatively small despite micrometer-scale roughness; they provide error bars for the E_F energies.

Table 1. AFM Roughness with KPFM CPD and Work Function Values, Φ, Valence and Conduction Band Edges, and Band-Gap Energies Measured by XPS and DRCLS

sample	CPD (mV)	Φ (eV)	error (eV)	E_V (eV)	E_C (eV)	E_g CL/UV−vis (eV)	average roughness (nm)	rms roughness (nm)
$CaTaO_2N$	165.38	−4.596	0.09	−5.81	−3.24	2.57/2.6	115	149
$SrTaO_2N$	368.53	−4.393	0.023	−5.99	−3.78	2.06/2.2	166	217
$BaTaO_2N$	193.07	−4.568	0.043	−6.03	−4.06	---/2.0	279	341
$PrTaON_2$	281.45	−4.479	0.116	−5.59	−3.56	1.92/2.0	190	238
HOPG	286.05	−4.475	0.005					

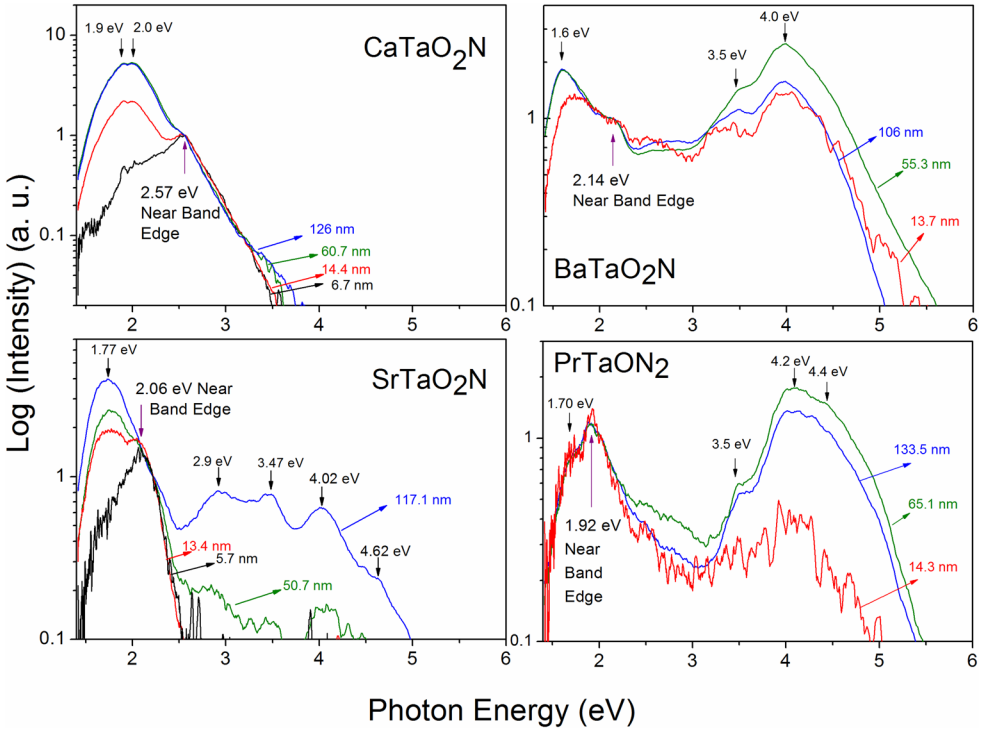

Figure 5. DRCL spectra of oxynitrides showing NBE and defect features at various probe depths. Peak features below NBE energies correspond to defect recombination.

dx.doi.org/10.1021/cm401815w | *Chem. Mater.* 2013, 25, 3337−3343

The DRCL spectra of $CaTaO_2N$ and $SrTaO_2N$ show emissions at energies 0.3 to 0.4 eV below the band gap that corresponds to defect-level recombination. These emissions are centered near 2.0 and 1.77 eV for $CaTaO_2N$ and $SrTaO_2N$, respectively. In both cases, the intensity of these emissions with respect to the I(NBE) increases with increasing E_B, indicating that the bulk of the sample has a higher level of defects than it does near the surface. It is possible to discern a sub-band gap emission at 1.70 eV in the DRCL spectra of $PrTaON_2$. However, unlike $CaTaO_2N$ and $SrTaO_2N$, the intensity of this emission with respect to the I(NBE) does not increase with the excitation depth, suggesting a lower level of defects in the bulk of the $PrTaON_2$ samples.

The DRCL spectra collected for $BaTaO_2N$ are more difficult to interpret. We know from the UV−vis spectra that the band gap should be in the 1.9−2.0 eV range, yet, unlike the other three samples, there is no clear near band edge peak, only a shoulder feature at 2.14 eV. Nor do the emissions drop off sharply for energies above the band edge, as with $SrTaO_2N$. The lack of a clear near band edge emission often indicates a relatively high concentration of defect states. The extended onset of UV−vis absorption also indicated defect states, presumably associated with nonstoichiometry in $BaTaO_2N$. Consequently, both spectroscopic probes indicated higher levels of defects in $BaTaO_2N$ than the other three compounds. As with $CaTaO_2N$ and $SrTaO_2N$, defect emissions with respect to the I(NBE) increased with the excitation depth. However, for this oxynitride, the near-surface DRCL spectrum was too weak to measure.

Figure 6 shows XPS valence band spectra of all four oxynitrides with their leading edges shown in parentheses. The inset shows the C1s core level spectra acquired concurrently for the same surfaces. C1s peak shifts reflect charging and rigid energy shifts. The $E_V - E_F$ values corrected for this charging appear in bold. The Figure 6 spectra are from only uniformly coated samples measured by AFM with the least amount of XPS charging. All samples exhibited charging as measured by the position of the C1s core level, as presented in the Figure 6 inset, with the exception of $BaTaO_2N$. Such charging is consistent with reports from other groups for similar compounds,[32] which is not unexpected because these materials are wide band gap semiconductors.

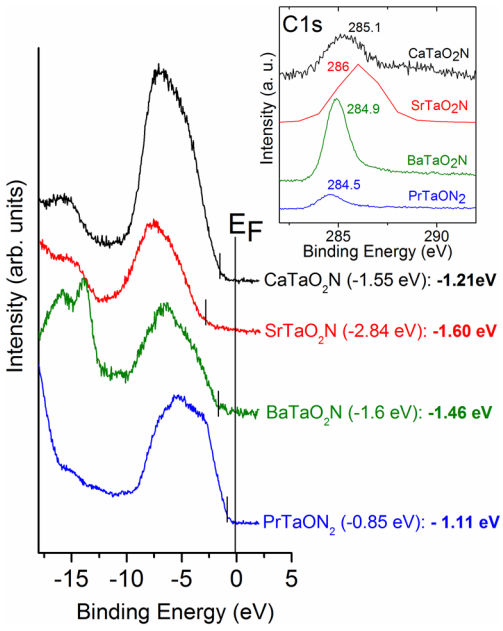

Figure 6. Valence bands of oxynitrides relative to E_F. The inset shows C1s taken concurrently. The short vertical lines indicate the extrapolated E_V (energies in parentheses) and E_V (bold) values corrected for charging. The system E_F was measured as −0.14 eV from the Au spectra.

All of the results described above have been combined in Table 1, which lists the average roughness, rms roughness, contact potential difference (CPD), and calculated work functions of the compounds measured by noncontact KPFM.[28,33] The CPD values in Table 1 represent the average potential values of several different spots taken on a sample, with the standard deviation as an error and their corresponding calculated absolute work functions.[33] The table also lists the band gap, valence, and conduction band energies.

4. DISCUSSION

Figure 7 compiles the DRCLS, KPFM, and XPS results and values listed in Table 1 into an energy-level diagram of all four

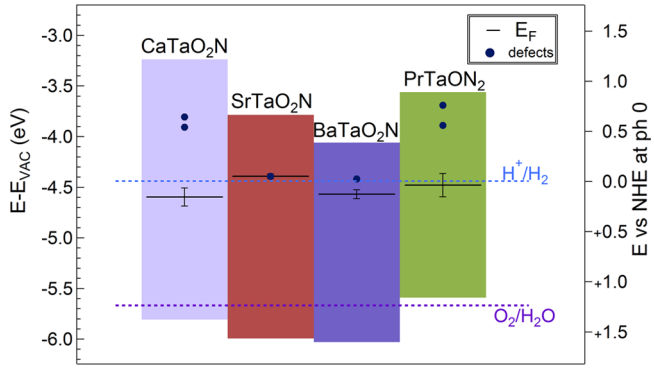

Figure 7. Energy-level diagrams of tantalum oxynitrides showing E_C and E_V as well as band gap (colored) and defect levels (●) obtained from XPS and DRCLS, E_F (heavy lines) obtained from KPFM, and H_2O redox potentials.

oxynitride compounds with respect to the vacuum level and relative to the redox potentials of water (−4.44 and −5.67 eV for reduction and oxidation, respectively). As mentioned above, the position of E_F was calculated from a CPD whose error (shown with error bars) adds into the position of E_V. As shown, the band gaps of $BaTaO_2N$, $SrTaO_2N$, and $CaTaO_2N$ increase as expected with decreasing cation size. For the Ba−Sr−Ca oxynitride series, the increasing band gap can largely be attributed to changes in the energy of the conduction band edge. As the size of the alkaline-earth cation decreases ($r_{Ca} < r_{Sr} < r_{Ba}$), the tilting of the octahedra increases (Figure 2), which narrows the conduction bands. The decreased dispersion of the conduction bands raises the energy of the conduction band edge and increases the band gap.[34−36] In contrast, the valence band edge positions of the $ATaO_2N$ compounds are relatively insensitive to the structural changes that accompany changes in the size of the alkaline earth cation, shifting slightly upward by only 0.2 eV on going from A = Ba to Ca.

Although the Ba−Sr−Ca series illustrates the effect of octahedral tilting on the electronic structure, a comparison of $CaTaO_2N$ and $PrTaON_2$ illustrates the effect of changing the oxygen-to-nitrogen ratio. Ca^{2+} and Pr^{3+} have nearly identical ionic radii (1.12 and 1.13 Å, respectively, for eightfold

dx.doi.org/10.1021/cm401815w | Chem. Mater. 2013, 25, 3337−3343

coordination);[37,38] therefore, the octahedral tilting in these two compounds is similar. In fact, the average Ta−(O/N)−Ta angles, which are characteristic of the degree of tilting, are similar (154.5(1)° for $CaTaO_2N$ and 156.2(1)° for $PrTaON_2$). However, the average Ta−O/N bond distance does expand from 2.027 ($CaTaO_2N$) to 2.052 Å ($PrTaON_2$) as the nitrogen content increases.[39] The net effect on the electronic structure appears to be a narrowing of the band gap resulting from shifts in both the valence and conduction band edge positions. To a first approximation, the longer Ta−O/N bond distances will make the conduction band minimum less antibonding and therefore lower in energy. The increased concentration of the more electropositive nitrogen is responsible for the upward shift in the valence band maximum. It is worth noting that Pr^{3+} has a $4f^2$ electron configuration, which means that transitions from the localized Pr 4f states to the conduction band can occur. However, the fact that $PrTaON_2$ and $LaTaON_2$[40] have similar colors and UV−vis spectra suggests that the 4f states are not located in the gap.

Previous work of Domen et al. using UV photoemission spectroscopy (UPS) and electrochemical analysis reported the valence band positions (E_V) relative to both the vacuum level (E_{VAC}) and Fermi level (E_F) of Ta_2O_5, TaON, and Ta_3N_5.[32] The authors of this work also determined conduction band levels using UV−vis diffuse reflectance spectroscopy to measure the semiconductors' absorption edge and hence their band gaps. They found that conduction band energies relative to E_{VAC} for all three materials are similar but their E_V levels vary significantly. Because oxynitride conduction bands are derived predominantly from Ta 5*d* orbitals and the O 2*p* and N 2*p* orbitals dominate in the valence band, it is perhaps not too surprising that the valence band edge is more sensitive to changes in the oxygen-to-nitrogen ratio than the conduction band edge. Theoretical studies indicate that the valence band maximum is expected to move higher (i.e., to a lower binding energy) with the replacement of O by N in oxynitrides.[41] This is born out in both our study (i.e., $CaTaO_2N$ vs $PrTaON_2$) and the earlier study on Ta_2O_5, TaON, and Ta_3N_5.

As shown by Maeda and Domen,[42] $CaTaO_2N$, $SrTaO_2N$, and $BaTaO_2N$ are active for photocatalytic H_2 evolution but not for O_2 evolution. The fact that hydrogen can be produced requires the conduction band edge to be located above the H^+/H_2 redox potential, which is consistent with the absolute band edge positions shown in Figure 7. At first glance, the inability of these compounds to photocatalytically produce oxygen is not necessarily consistent with the band edge positions shown in Figure 7. However, the valence band edges are only slightly below the H_2O/O_2 redox potential, which means that there is little excess driving energy to overcome even relatively small activation barriers for the four-hole oxidation of water. The results show that the valence band edge position of $PrTaON_2$ is such that it cannot produce oxygen but, as a hydrogen evolution photocatalyst in a tandem or *Z*-scheme system, it has a conduction band edge position that is more favorable than that of $BaTaO_2N$ despite the fact that both compounds have similar band gaps. Maeda and Domen[43] also show that $BaZrO_3$−$BaTaO_2N$ has a possibility for overall water splitting into both H_2 and O_2, which agrees with the absolute band position in Figure 7 where $BaTaO_2N$ is most likely to yield O_2 evolution.

Figure 7 also shows the defect-level energies obtained from DRCLS within the band gaps of these oxynitrides. States near midgap have the highest cross section for acting as recombination centers and thereby decreasing photocatalytic efficiency.[44] Although it is not possible in this study to unambiguously identify the defects responsible for these emissions, it is likely that the defects are native point defects. Although such defects are present in all compounds, their concentration appears to be the highest in $BaTaO_2N$. In spite of the fact that DRCLS is not a tool accessible to most researchers, there appears to be a correlation between the presence of sub-band gap absorption as detected in the UV−vis measurements and high levels of cathodoluminescence. This is worth noting because most researchers can collect UV−vis spectra. $BaTaO_2N$ and $PrTaON_2$ have very similar band gaps and thus absorb a similar fraction of the visible spectrum. However, $PrTaON_2$ has a lower level of sub-band gap defects, and its conduction band edge lies at a higher energy. Both features may make this material, reported here for the first time, a potentially better option for use in *Z*-scheme photocatalysis.

5. CONCLUSIONS

We have used a combination of DRCLS, XPS, AFM, and KPFM to determine the absolute conduction and valence band energies of the tantalum oxynitride series $ATaO_2N$ (A = Ca, Sr, and Ba) and $PrTaON_2$. These oxynitrides were prepared by growth methods that yield relatively smooth, uniform, and low-charging surfaces and were suitable for electronic property measurements. The valence and conduction band edges for the $ATaO_2N$ series vary systematically. The position of the conduction band edge can be tuned by changing the size of the A-site cation. Smaller A-site cations lead to more octahedral tilting and less disperse conduction bands and thus a higher energy for the conduction band edge. The position of the valence band edge can be tuned by varying the oxygen-to-nitrogen ratio. Increasing the nitrogen content leads to an upward shift in the position of the valence band edge.

AUTHOR INFORMATION

Notes

The authors declare no competing financial interest.

ACKNOWLEDGMENTS

P.M.W and S.P. acknowledge partial support from the National Science Foundation, award no. DMR-0907356. The authors acknowledge partial support by the Center for Emergent Materials at The Ohio State University under NSF MRSEC award no. DMR-0820414.

REFERENCES

(1) Yamasita, D.; Takata, T.; Hara, M.; Kondo, J. N.; Domen, K. *Solid State Ionics* **2004**, *172*, 591.
(2) Liu, M.; You, M.; Lei, Z.; Takata, T.; Domen, K.; Li, C. *Chin. J. Catal.* **2006**, *27*, 556.
(3) Fujishima, A.; Honda, K. *Nature* **1972**, *238*, 37.
(4) Maeda, K.; Domen, K. *J. Phys. Chem. C* **2007**, *111*, 7851.
(5) Kudo, A.; Miseki, Y. *Chem. Soc. Rev.* **2007**, *38*, 253.
(6) Kurihara, T.; Okutomi, H.; Miseki, Y.; Kato, H.; Kudo, A. *Chem. Lett.* **2006**, *35*, 274.
(7) Kato, H.; Kudo, A. *Chem. Phys. Lett.* **1998**, *295*, 487.
(8) Kato, H.; Asakura, K.; Kudo, A. *J. Am. Chem. Soc.* **2003**, *125*, 3082.
(9) Sayama, K.; Arakawa, H. *J. Photochem. Photobiol., A* **1994**, *77*, 243.
(10) Yoshino, M.; Kakihana, M.; Cho, W. S.; Kato, H.; Kudo, A. *Chem. Mater.* **2002**, *14*, 3369.

(11) Otsuka, H.; Kim, K.; Kouzu, A.; Takimoto, I.; Fujimori, H.; Sakata, Y.; Imamura, H.; Matsumoto, T.; Toda, K. *Chem. Lett.* **2005**, *34*, 822.
(12) Ebbinghaus, S. G.; Abicht, H.-P.; Dronskowski, R.; Muller, T.; Reller, A.; Weidenkaff, A. *Prog. Solid State Chem.* **2009**, *37*, 173.
(13) Fuertes, A. *J. Mater. Chem.* **2012**, *22*, 3293.
(14) Hitoki, G.; Takata, T.; Kondo, J. N.; Hara, M.; Kobayashi, H.; Domen, K. *Chem. Commun.* **2002**, 1698.
(15) Tsang, M.-Y.; Pridmore, N. E.; Gillie, L. J.; Chou, Y.-H.; Brydson, R.; Douthwaite, R. E. *Adv. Mater.* **2012**, *24*, 3406.
(16) Nakhal, S.; Lumey, M.-W.; Bredow, T.; Dronskowski, R.; Lerch, M. *Z. Anorg. Allg. Chem.* **2010**, *636*, 1006.
(17) Oro-Sole, J.; Clark, L.; Bonin, W.; Attfield, J. P.; Fuertes, A. *Chem.Comm.* **2013**, *49*, 2430.
(18) Lu, Y.; Le Paven-Thivet, C.; Benzerga, R.; Le Gendre, L.; Sharaiha, A.; Tessier, F.; Chevire, F. *Appl. Surf. Sci.* **2013**, *264*, 533.
(19) Sierra Gallego, G.; Marin Alzate, N.; Arnache, O. *J. Alloys Compd.* **2013**, *549*, 163.
(20) Park, W. B.; Jeong, Y. S.; Singh, S. P.; Sohn, K.-S. *ECS J. Solid State Sci. Technol.* **2013**, *2*, R3100.
(21) Higashi, M.; Abe, R.; Teramura, K.; Takata, T.; Ohtani, B.; Domen, K. *Chem. Phys. Lett.* **2008**, *452*, 120.
(22) Kim, Y.-I.; Woodward, P. M.; Baba-Kishi, K. Z.; Tai, C. W. *Chem. Mater.* **2004**, *16*, 1267.
(23) Hou, B.; Li, Z.; Xu, Y.; Wu, D.; Sun, Y. *Chem. Lett.* **2005**, *34*, 1040.
(24) Hovington, P.; Drouin, D.; Gauvin, R. *Scanning* **1997**, *19*, 1.
(25) (a) Brillson, L. J. *J. Vac. Sci. Technol., B* **2001**, *19*, 1762. (b) Brillson, L. J. *J. Phys. D: Appl. Phys.* **2012**, *45*, 183001.
(26) Yacobi, B. G.; Hol, D. B. *J. Appl. Phys.* **1986**, *59*, R1.
(27) Liu, Y.; Shen, S.; Brillson, L. J.; Gordon, R. G. *Appl. Phys. Lett.* **2011**, *98*, 122907.
(28) Walsh, S.; Fang, L.; Schaeffer, J. K.; Weisbrod, E.; Brillson, L. J. *Appl. Phys. Lett.* **2007**, *90*, 052901.
(29) Drouin, D.; Couture, A. R.; Joly, D.; Tastet, X.; Aimez, V.; Gauvin, R. *Scanning* **2007**, *29*, 92.
(30) Pankove, J. I. In *Optical Processes in Semiconductors*; Holonyak, N., Jr., Ed.; Prentice-Hall: Englewood Cliffs, NJ, 1971; p 12.
(31) van Benthem, K.; Elsasser, C.; French, R. H. *J. Appl. Phys.* **2001**, *90*, 6156.
(32) Chun, W.-J.; Ishikawa, A.; Fujisawa, H.; Takata, T.; Kondo, J. N.; Hara, M.; Kawai, M.; Matsumoto, Y.; Domen, K. *J. Phys. Chem. B.* **2003**, *107*, 1798.
(33) Rosenwaks, Y.; Shikler, R.; Glatzel, Th.; Sadewasser, S. *Phys. Rev. B* **2004**, *70*, 085320.
(34) Lufaso, M. W.; Woodward, P. M. *Acta Crystallogr., Sect. B* **2001**, *57*, 725.
(35) Mizoguchi, H.; Eng, H. W.; Woodward, P. M. *Inorg. Chem.* **2004**, *43*, 1667.
(36) Eng, H. W.; Barnes, P. W.; Auer, B. M.; Woodward, P. M. *J. Solid State Chem.* **2003**, *96*, 535.
(37) Shannon, R. D. *Acta Crystallogr.* **1976**, *A32*, 751.
(38) Jia, Y. Q. *J. Solid State Chem.* **1991**, *95*, 184.
(39) Porter, S. H. Perovskite and Pyrochlore Tantalum Oxide Nitrides: Synthesis and Characterization. M.S. Thesis, The Ohio State University, Columbus, OH, 2012.
(40) Park, N.-Y.; Kim, Y.-I. *J. Mater. Sci.* **2012**, *47*, 5333.
(41) Fang, C. M.; Orhan, E.; de Wijs, G. A.; Hintzen, H. T.; Groot, R. A.; Marchand, R.; Saillard, J.-Y.; de With, G. *J. Mater. Chem.* **2001**, *11*, 1248.
(42) Maeda, K.; Domen, K. *MRS Bull.* **2011**, *36*, 25.
(43) (a) Maeda, K.; Domen, K. *Angew. Chem., Int. Ed.* **2012**, *51*, 9865. (b) Maeda, K.; Domen, K. *J. Catal.*, in press.
(44) Bhattacharya, P. *Semiconductor Optoelectronic Devices*; Prentice Hall: Upper Saddle River, NJ, 1997; pp 103−106.